Journal of the European Ceramic Society **16** (1996) 203–209

0955-2219(95)00132-8
0955-2219/96/$15.00

EXAFS Studies of Cr-doped Mullite

K. R. Bauchspieß,[a,*] H. Schneider[b] & A. Kulikov[c]

[a]School of Mathematical and Physical Sciences, Murdoch University, Perth, WA 6150, Australia
[b]German Aerospace Research Establishment (DLR), Institute for Materials Research, D-51140 Köln, Germany
[c]Institute of Chemistry, Russian Academy of Sciences, Vladivostok 690022, Russia

(Accepted 22 July 1995)

Abstract

Mullites doped with 7·3 (Cr 6) and 11·5 wt% Cr_2O_3 (Cr 10) were synthesized by reaction sintering of Al_2O_3, SiO_2 and Cr_2O_3 powder compacts at 1650°C in air. Prior to the spectroscopic analyses, the powder samples were HF/HCl-washed in order to remove coexisting glassy phases. According to X-ray diffractometry all samples consisted of mullite only.

Measurements of the extended X-ray absorption fine structure (EXAFS) of the Cr K edge of mullite were performed at the Photon Factory, National Laboratory of High Energy Physics (KEK), in Tsukuba, Japan. The measured spectra were normalized by first subtracting a pre-edge background and then fitting a smoothly varying cubic-spline background in the region of the EXAFS. For all measured spectra the magnitude of the Fourier transform, which is related to the pair distribution function (PDF) and similar to it, is characterized by two pronounced peaks. The first peak is ascribed to oxygen making up the octahedra surrounding the Cr atoms and the second peak is assumed to be due to Al. It turned out that the second peak could not be fitted satisfactorily with one Al coordination shell alone. The discrepancy can be reduced by assuming that there is an additional contribution from Cr atoms that do not occupy regular lattice sites but are displaced by some amount. The existence of such displaced Cr atoms is known from EPR and crystal field spectroscopy experiments. Since these Cr atoms are not in the center of the Al coordination shell, the Al PDF seen by these Cr atoms is broadened and also slightly asymmetric. From our data analysis we find the displacement of the Cr atoms from the center of their surrounding aluminum coordination shell to be 0·50 Å.

1 Introduction

Mullite has the general composition $Al_{4+2x}Si_{2-2x}O_{10-x}$ ($0{\cdot}25 \leq x \leq 0{\cdot}4$).[1] The orthorhombic crystal structure of mullite contains chains of edge sharing AlO_6 octahedra running parallel to the crystallographic *c*-axis. Octahedral columns are crosslinked by tetrahedra double chains with randomly distributed Al and Si atoms. Tetrahedra double chains also run parallel to *c*. Some O atoms bridging adjacent tetrahedra are removed and as a consequence a new tetrahedral site is formed, in which the bridging O atoms belong to three tetrahedra (e.g. Refs 2–4).

Earlier work on the doping of mullite with Cr was performed by Gelsdorf *et al.*,[5] Murthy and Hummel,[6] and Rager *et al.*.[7] It has been stated that up to 12 wt% Cr_2O_3 is incorporated in mullite. A detailed study of the crystal chemistry of Cr-doped mullites prepared by reaction sintering of Al_2O_3, SiO_2 and Cr_2O_3 (0·5–11 wt%) powders, was performed by Rager *et al.*.[13] Rager *et al.* found a reciprocal and equimolar dependence between Cr_2O_3 and Al_2O_3 in mullite, but not between Cr_2O_3 and SiO_2 contents. They concluded that Cr^{3+} is incorporated by replacement of Al^{3+}. The structural state (*x*-value) of Cr-doped mullite, which corresponds to that of 3/2-type mullite, indicates that the variation of Cr incorporation is not correlated with a change of the amount of O(C) oxygen vacancies in mullite.

Electron paramagnetic resonance (EPR) studies provided information on the structural distribution of Cr in mullite:[7] Cr-doped mullites exhibit two sharp EPR signals near $g_{eff} = 5$, and a broad signal near $g_{eff} = 2{\cdot}2$. The peaks near $g_{eff} = 5$ were assigned to Cr^{3+} in slightly distorted octahedral Al chain positions in mullite. The broad, slightly asymmetric signal near $g_{eff} = 2{\cdot}2$ may indicate coupling between localized magnetic moments, and was associated with interstitial Cr^{3+} incorporation in mullite. According to the EPR peak intensities the entry of Cr^{3+} into the regular AlO_6 octahedra is favoured at low bulk Cr_2O_3 contents of mullite, whereas interstitial incorporation with formation of Cr clusters becomes more important at higher Cr_2O_3 contents. Unpolarized crystal field spectra

*To whom correspondence should be addressed.

measured by Ikeda *et al.*[8] in the wavelength range from 340 to 1540 nm by reflection from mullite powders with about 8 wt% Cr_2O_3 yielded further evidence for the structural distribution model of Cr^{3+} developed by Rager *et al.*[7]

2 Sample Material

Samples were prepared from about 4 g of chemically pure Al_2O_3(VAW, 302), SiO_2 (Ventron, 88316), and Cr_2O_3 (Merck, 2483) powders, with 62–x wt% Al_2O_3, 38 wt% SiO_2, and x wt% Cr_2O_3 (x = 6, 10; designated as samples Cr 6 and Cr 10). The mixtures were pressed into disks of 20 mm diameter and 5 mm thickness in a pressing mold using uniaxial pressure loading, in a laboratory furnace in air at 1650°C. Prior to the EXAFS measurements the samples were HF/HCl-washed in order to leach the coexisting glassy phase. According to X-ray diffractometry all HF/HCl-treated samples consisted of mullite only. The actual chemical compositions of acid washed mullites determined by microprobe analysis were: Cr 6: Al_2O_3: 64·1 wt%, SiO_2: 28·5 wt%, C_2O_3: 7·3 wt%, and Cr 10: Al_2O_3: 60·0 wt%, SiO_2: 28·4 wt%, Cr_2O_3: 11·5 wt % (see Ref. 7).

3 EXAFS Measurements

3.1 Basic considerations

EXAFS spectroscopy measures the pair distribution function with respect to the absorbing atom as center. The pair distribution function $P(R)$ about the X-ray absorbing atom is defined through

$$N(R) = 1 + \int_0^R P(\tilde{R})\, \mathrm{d}\tilde{R} \tag{1}$$

$N(R)$ is the number of atoms contained in a sphere of radius R centered at the X-ray absorbing atom. Hence, integrating $P(R)$ yields the number of atoms in the system. (The radial distribution function $g(R)$ is obtained via $g(R) = P(R)/(4\pi v R^2)$, where v is the number density.) In a solid the atoms can be grouped in coordination shells about a given atom and $P(R)$ can be written as a sum over S coordination shells:

$$P(R) = \sum_{j=1}^{S} P_j(R) \tag{2}$$

The EXAFS function, $\chi(k)$, is given by the following expression:

$$\chi(k) = S_0^2 \cdot \sum_{j=1}^{S} \frac{1}{k_j} \int_0^\infty \frac{\mathrm{dR}}{R^2} \,|f_{b,j}(k_j, R, \pi)| \cdot \exp \tag{3}$$

$$(-2R/\lambda_j(k_j)) \cdot P_j(R) \cdot \sin(2k_jR + \delta_c(k_j) + \delta_{b,j}(k_j, R, \pi))$$

R is the distance from the absorbing atom (Cr) and k_j is the magnitude of the wavevector of the photoelectron. The atoms of different coordination shells may experience different potentials and therefore the photoelectron wavevector k_j of a coordination shell must be adjusted. k_j is related to the wavevector k of the data by means of an adjustable energy shift ΔE_j:

$$k_j = \sqrt{k^2 - \Delta E_j/\gamma} \text{ with } \gamma \equiv \frac{h^2}{8\pi^2 m_e} \cong 3{\cdot}81 \text{ eVÅ}^2 \tag{4}$$

$|f_{b,j}(k_j, R, \pi|$ and $\delta_{b,j}(k_j, R, \pi)$ are magnitude and phase of the complex backscattering amplitudes $f_{b,j}(k_j, R\pi)$, and $\delta_C(k_j)$ is the central-atom phaseshift (of Cr) for K-shell absorption. $\lambda_j(k_j)$ is the inelastic mean free path of the photoelectron. S_0^2 is an overall amplitude reduction factor due to multi-electron excitations. Since the R-dependence of $f_{b,j}(k_j, R, \pi)$ is weak, R can be replaced by its average value R_j for shell j, as far as the backscattering amplitude is concerned, and eqn (3) becomes:

$$\chi(k) = S_0^2 \cdot \sum_{j=1}^{S} \frac{|f_{b,j}(k_j, R_j, \pi)|}{k_j} \int_0^\infty \frac{\mathrm{d}R}{R^2} \exp$$

$$(-2R/\lambda_j(k_j)) \cdot P_j(R) \cdot \sin(2k_jR + \delta_c(k_j) + \delta_{b,j}(k_j, R_j, \pi)) \tag{5}$$

In the harmonic approximation it is assumed that the pair distribution functions $P_j(R)$ are Gaussians:

$$P_j(R) = \frac{N_j}{\sigma_j \sqrt{2\pi}} \exp(-(R-R_j)^2/2\sigma_j^2) \tag{6}$$

N_j is the number of atoms in shell j. Inserting eqn (6) into eqn (5) one obtains the standard EXAFS formula:

$$\chi(k) = S_0^2 \cdot \sum_{j=1}^{S} \frac{N_j}{k_j R_j^2} |f_{b,j}(k_j, R_j, \pi)| \cdot \exp(-2R_j/\lambda_j(k_j))$$

$$\cdot \exp(-2\sigma_j^2 k_j^2) \cdot \sin(2k_jR_j + \delta_c(k_j) + \delta_{b,j}(k_j, R_j, \pi)) \tag{7}$$

From the measured EXAFS data one can obtain a first guess at the pair distribution function by calculating the Fourier transform. This is done according to:

$$H(R) = \frac{1}{\sqrt{\pi}} \int_{-\infty}^{\infty} w(k)\chi(k)k^p e^{+i2kR} \mathrm{d}k \tag{8}$$

Here the term k^p was introduced in order to compensate for the decrease of $\chi(k)$ with k. $w(k)$ is a Hamming window function[9] and is applied in

order to suppress sidelobes in the Fourier transform. $w(k)$ vanishes everywhere except on the interval $k_{min} \leq k \leq k_{max}$ where it is given by:

$$w(k) = 0{\cdot}54 + 0{\cdot}46 \cos(2\pi k/\Delta k) \text{ with } \Delta k = k_{max} - k_{min} \quad (9)$$

$H(R)$ is a complex function whose magnitude is related, but not equal, to the pair distribution function. In order to extract quantitative information from the data one has to employ curve fitting techniques.

3.2 Experimental procedure

The EXAFS experiments were carried out at Beamline 7C of the Photon Factory, National Laboratory for High Energy Physics, Japan. The positron storage ring was operating at 2·5 GeV and had a beam lifetime of about 70 h. The average positron current during the measurements was 270 mA. Measurements of the Cr K edge EXAFS were performed on mullite samples doped with 7·3 and 11·5 wt% Cr_2O_3 (samples Cr 6 and Cr 10, see Section 2). Samples with an absorption thickness product of about 2 in the region just after the edge were mounted on Scotch Tape. The spectra were measured in transmission, with the first ion chamber filled with N_2 gas and the second filled with a mixture of 25% Ar and 75% N_2. In order to suppress harmonics in the X-ray beam the Si(111) double-crystal monochromator was detuned from parallelism such that the output intensity decreased by at least 50%.

4 Results of EXAFS Data Analysis

The EXAFS was extracted from the measured X-ray absorption spectra by normalizing the spectra in the usual way. First, the pre-edge region was fitted to a Victoreen-type background: $A_0 + A_3/E^3 + A_4/E^4$. E is the X-ray energy. The background was then extended into the edge and post-edge region and subtracted from the whole spectrum.

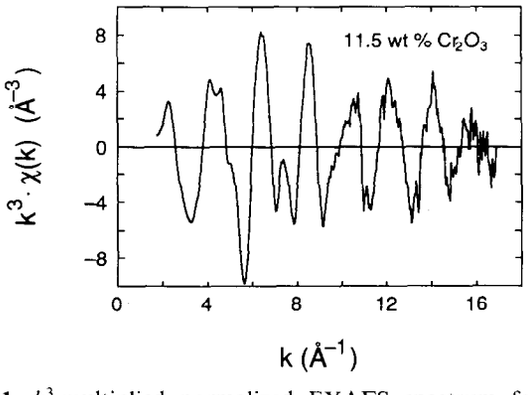

Fig. 1. k^3-multiplied normalized EXAFS spectrum for the Cr 10 sample (~11·5 wt% Cr_2O_3) measured at 300 K.

After converting the spectrum above the energy E_{edge} of the absorption edge to the wavevector scale k according to $k = \sqrt{(E - E_{edge}) \cdot 8\pi^2 m_e / h^2}$ a second background was fitted to the EXAFS region of the spectrum. This background consisted of a smoothing spline $s(k)$ using cubic polynomials[10]. The EXAFS, $\chi(k)$ was then obtained by forming the difference between the data $y(k)$ and the background and dividing by the height D of the absorption step at the edge: $\chi(k) = (y(k)-s(k))/D$. One such normalized spectrum is shown in Fig. 1. The spectrum has been multiplied by k^3 in order to compensate for the decrease of the envelope with k. The data analysis is carried out using three different models, labelled 1, 2 and 3 and described below.

4.1 Model 1

For the samples investigated in this work, the magnitude of the Fourier transform, calculated according to eqn (8) and for $p = 3$, is dominated by two peaks (Fig 2(a)). The first peak is due to the nearest-neighbour (NN) O atoms that surround the Cr atoms. The second peak is assumed

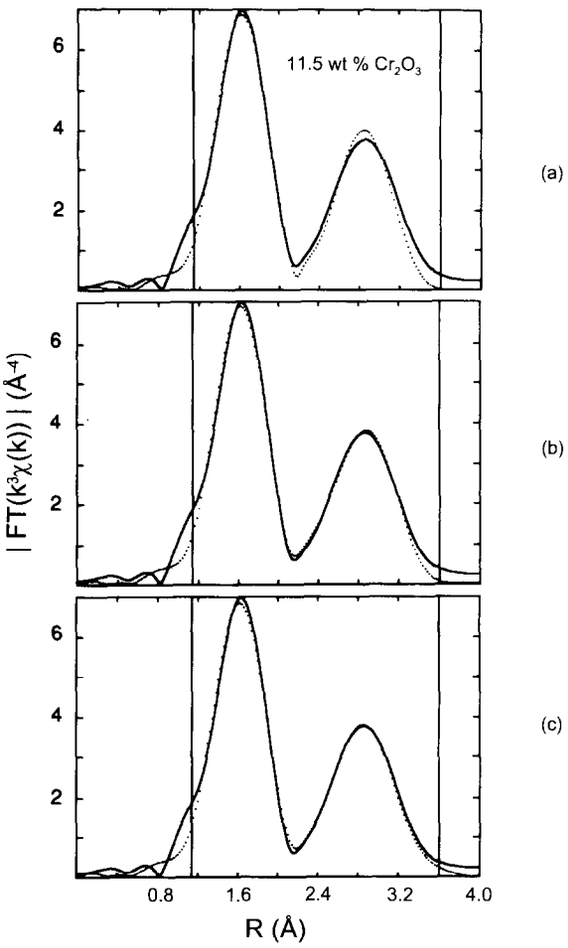

Fig. 2. Fourier transform magnitude for the Cr 10 sample (~11·5 wt% Cr_2O_3) measured at 300 K (solid line) and fit data (dotted line) from a simultaneous fit to three datasets: (a) with two coordination shells (O and Al) each; (b) with three coordination shells each; (c) with three coordination shells each, but taking the displacements of Cr atoms explicitly into account.

to be due to a next-nearest neighbour (NNN) coordination shell consisting of Al and/or Si atoms. It is impossible in EXAFS spectroscopy to distinguish between backscattering from Al and from Si atoms because Al and Si are too close in atomic number. Hence, it was assumed that the NNN coordination shell consisted of Al atoms only. In order to obtain quantitative information, the O and Al shells were curve fitted using a program developed by one of the authors.[11] The spectra were first fitted according to the standard EXAFS formula (eqn 7). Amplitudes and phases of the shells were calculated using the single-scattering version of the FEFF code (version 3.1.1).[12] In a fit using the harmonic approximation there are four parameters that can be varied for each coordination shell: ΔE_j, R_j, σ_j^2 and N_j. Least-squares fits to both coordination shells were carried out simultaneously to the real and imaginary parts of the Fourier transform. The Fourier transform of $k^3\chi(k)$, with $\chi(k)$ according to eqn (7), was fitted to the Fourier transform of the k^3-multiplied data. The data that was fitted was for the Cr10 sample measured at 300 and at 150 K, and for the Cr 6 sample measured at 300 K. Three such datasets were fitted in real space simultaneously. By fitting multiple spectra one is able to include constraints on the fitting parameters and reduce the number of variable parameters per dataset. For example, one can exploit the fact that the energy corrections ΔE are identical for each atom type and that the coordination numbers are temperature independent. A typical fit carried out in this way is shown in Fig. 2. The fit interval is indicated by the vertical lines, and 16 variable fit parameters were employed for the simultaneous fit to three datasets with two shells each. There is a shoulder, which could not be fitted, at about 1 Å at the low R side of the oxygen peak. Assuming two oxygen shells could not reduce the discrepancy and thus only one O shell will be used.

The spectra had been fitted ignoring the amplitude reduction factor S_0^2. Therefore, the coordination numbers had come out too low. From the absence of a peak just before the Cr K absorption edge one knows that the immediate Cr environment has inversion symmetry[13] and one can thus assume that each Cr atom is octahedrally coordinated. With 6 oxygen atoms around each Cr atom, but only 4.3 atoms obtained from the data analysis, we conclude that for the data in Table 1 S_0^2 = 0·72. Values of S_0^2 are usually around 0·7. For Fe, which is near to Cr in the periodic table, a value of 0·69 is reported.[14] Using S_0^2 = 0·72 one obtains for the Al coordination numbers N_{Al} = 6·9.

Special attention has been given to error estimation. Using a method outlined in Ref. 15, the error of a variable parameter in an n parameter fit was determined by giving this parameter fixed values around the optimum and for each given value performing an n–1 parameter fit with the remaining fit parameters. This method is computationally intensive but properly takes into account all parameter correlations. The error bars were obtained from the width of the minima of the residual sums of squares (χ^2) curves. In order determine up to which value χ^2_{max} along each χ^2 curve to go, it is assumed that the error for ΔE_O for the first coordination shell (O) is ± 1·0 eV. This determines χ^2_{max} and all other errors are then determined from the parameter values where χ^2 becomes equal to χ^2_{max}. For S_0^2 the error is determined from the fit error for the number N_O of atoms in the first coordination shell (O). All error bars were found to be approximately symmetric. The error bars given here do not include systematical deviations resulting from the procedure of calculating the scattering phases and amplitudes. Hence the EXAFS results are precise but not necessarily accurate. The methods described here to estimate S_0^2 and to determine the errors of the fit parameters are used throughout this work.

Table 1. Results of a simultaneous fit to three datasets with two coordination shells each

	R_O ΔR_O (Å)	σ_O^2 $\Delta\sigma_O^2$ (10^{-4} Å^2)	N_O ΔN_O	R_{Al} ΔR_{Al} (Å)	σ_{Al}^2 $\Delta\sigma_{Al}^2$ (10^{-4} Å^2)	N_{Al} ΔN_{Al}
7·3 wt%	1·985	34	6	3·258	42	6·9
300 K	±0·004	±4	±0	±0·007	±7	±0·6
11·5 wt%	1·984	33	6	3·261	47	6·9
300 K	±0·004	±4	±0	±0·007	±7	±0·6
Cr 10	1·984	28	6	3·258	36	6·9
150 K	±0·004	±4	±0	±0·006	±6	±0·6

ΔE_O = 0·6 eV ± 1·0 eV; ΔE_{Al} = −10·4 eV ± 1·1 eV; S_0^2 = 0·72 ± 0·04.

The PDF that is shown in Fig. 3(a) was calculated according to eqn (6) and corresponds to the fit shown in Fig. 2(a). The position of the Al peak (~3·26 Å) corresponds to Cr atoms occupying regular lattice sites in the mullite structure. Closer inspection of the data reveals that the second peak (Al) is not fitted very well. This is not because only Al, and not also Si, was considered here. Instead, the discrepancy might be due to asymmetry in the pair potential of Cr and Al atoms. A cumulant analysis,[16] including C_3 for the phase and C_4 for the amplitude, was attempted. However, no conclusive results could be obtained because there was not enough EXAFS signal available at the high-k end of the spectrum (Fig. 1), which is important for determining any cumulant terms. Considering the possible presence of other Cr atoms in the vicinity of the Cr absorber could

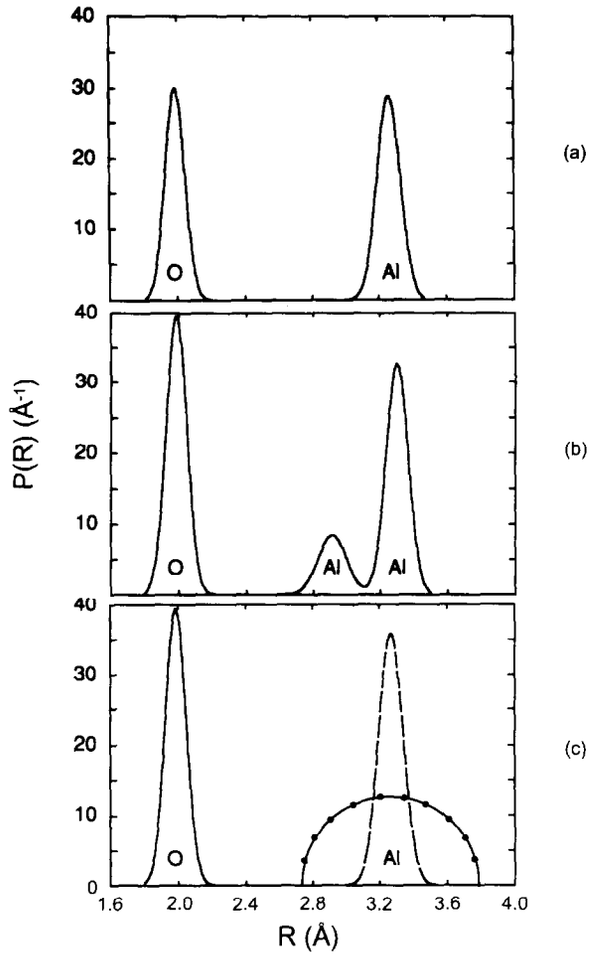

Fig. 3. Pair distribution function corresponding: (a) to the fit shown in Fig. 2(a); (b) to the fit shown in Fig. 2(b); (c) to the fit shown in Fig. 2(c); dashed line: Cr atoms in regular Al(1) sites, dotted line: Cr atoms in random interstitial sites.

not explain the discrepancy either and thus it had to be accounted for in other ways.

4.2 Model 2

The discrepancy can be reduced by including a third coordination shell, also consisting of Al atoms and close to the other Al shell. Again, three datasets were fitted simultaneously and the number of variable parameters is reduced by incorporating the constraints that all energy corrections ΔE are identical for each atom type and that the coordination numbers of each coordination shell are the same for each dataset, that is, the coordination numbers are assumed to be independent of temperature and of Cr_2O_3 content. The simultaneous fit to three spectra, with three coordination shells each, had then 23 variable parameters for the 9 coordination shells. The fit for the Cr 10 sample measured at 300 K is shown in Fig. 2(b) and the fit results are listed in Table 2.

Comparing these results with those shown in Table 1 one finds that the total number of Al atoms about the absorbing Cr atoms is almost the same (7·2 compared to 6·9) except that they are now distributed over two coordination shells. Figure 3(b) shows the PDF corresponding to the fit of Fig. 2(b). The Al peak at ~2·9 Å probably describes the environment of the interstitial Cr atoms and the Al peak at ~3.3 Å describes the environment of the Cr atoms at the regular lattice sites. The asterisks in place of error bars for σ^2_{Al} and N_{Al} for the coordination shell at ~2·9 Å indicate that the error was either very large or that it could not be determined because the minima of the χ^2 curves for σ^2_{Al} and N_{Al} were too shallow. This means that σ^2_{Al} and N_{Al} for the first Al coordination shell are not well defined.

For the 11·5 wt% Cr_2O_3 sample it can be seen from the table that the radius of the first Al shell decreases with increasing temperature. This anomalous behaviour could indicate an asymmetric PDF. However, taking asymmetry for this Al coordination shell into account is not practical because the correlation of the fit parameters becomes too large.

4.3 Model 3

In a third model, we now consider besides the Cr atoms occupying regular lattice sites, the effect of a large disorder of the interstitial Cr positions. These Cr atoms, with their *NN* oxygen octahedra, are assumed to be surrounded by an Al coordination shell of radius R_O but the average position of the Cr–O octahedra is off center by an amount $\zeta(\zeta \geq 0)$ as indicated in Fig. 4. The Al atoms are assumed to be continuously distributed over the coordination shell indicated in the figure. Neglecting atomic

Table 2. Results of a simultaneous fit to three datasets with three coordination shells each

	R_O ΔR_O (Å)	σ^2_O $\Delta\sigma^2_O$ (10^{-4} Å^2)	N_O ΔN_O	R_{Al} ΔR_{Al} (Å)	σ^2_{Al} $\Delta\sigma^2_{Al}$ (10^{-4} Å^2)	N_{Al} ΔN_{Al}	R_{Al} ΔR_{Al} (Å)	σ^2_{Al} $\Delta\sigma^2_{Al}$ (10^{-4} Å^2)	N_{Al} ΔN_{Al}
7·3 wt%	1·985	37	6	2·92	64	1·8	3·30	40	5·4
300 K	±0·004	±4	±0	±0·04	*	*	±0·02	±20	±1·6
11·5 wt%	1·984	37	6	2·91	73	1·8	3·30	40	5·4
300 K	±0·004	±4	±0	±0·04	*	*	±0·02	±20	±1·6
11·5 wt%	1·984	31	6	2·93	54	1·8	3·29	35	5·4
150 K	±0·004	±4	±0	±0·03	*	*	±0·02	±15	±1·6

ΔE_O = 0·6 eV ± 1·0 eV; ΔE_{Al} = –3 eV ± 3 eV; S_0^2 = 0·76 ± 0·04.

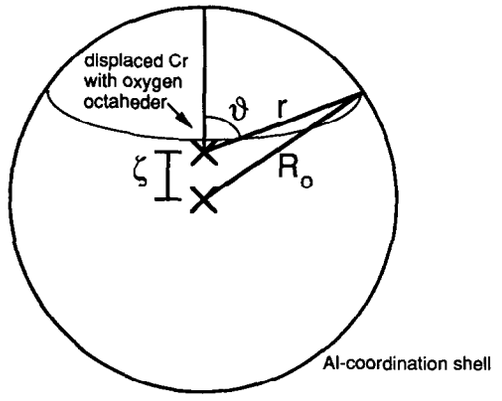

Fig. 4. Sketch of the displaced Cr atoms, octahedrally coordinated by six O atoms, but displaced from the center of the coordination sphere by the amount ζ. The Al atoms are assumed to be distributed continuously over the sphere.

vibrations for the moment, the distribution for the interstitial (displaced) Cr atoms ranges from $r = R_0 - \zeta$ to $r = R_0 + \zeta$. The number of Al atoms at distance r from a Cr atom displaced with its oxygen octahedra by ζ from the center of the Al coordination shell is proportional to the length $2\pi r \sin\vartheta(r)$ of the circle subtended by the angle ϑ (Fig. 4). The PDF for the Al atoms about the Cr atoms displaced by ζ is then:

$$P^*(r) = N_{Al} \frac{2\pi r \sin\vartheta(r)}{2\pi \int_{R_0-\zeta}^{R_0+\zeta} r \sin\vartheta(r)\, dr} \quad (10)$$

$$; \quad R_0 - \zeta \le r \le R_0 + \zeta \; ; \; \zeta \ge 0$$

The denominator is a normalization constant so that the total number of Al atoms in the coordination shell is N_{Al}. By eliminating $\vartheta(r)$, $P^*(r)$ can be brought into the form:

$$P^*(r) = N_{Al} \cdot \frac{1}{C} \cdot \frac{1}{\sqrt{[1 - (r - R_0)^2/\zeta^2] \cdot [(r + R_0)^2/\zeta^2 - 1]}} \quad (11)$$

where the normalization constant C is given by:

$$C = \int_{R_0-\zeta}^{R_0+\zeta} \sqrt{[1 - (r - R_0)^2/\zeta^2] \cdot [(r + R_0)^2/\zeta^2 - 1]}\, dr \quad (12)$$

The function $P^*(r)$ looks like a slightly asymmetric semicircle and is very broad compared to Gaussian widths. No disorder of the Al atoms, which will modify $P^*(r)$, has been considered because its effect will only lead to a negligible broadening of $P^*(r)$. The same applies to the distribution of ζ values. This was confirmed by numerically convolving $P^*(r)$ with distributions for R_O and ζ. Hence, $P^*(r)$ is employed as in eqns (11) and (12), without any convolution. Since $P^*(r)$ is not Gaussian the harmonic approximation cannot be used and eqn (5) is employed instead in order to calculate the EXAFS corresponding to $P^*(r)$. In addition to the constraints imposed for the previous model it is assumed that the ratio of ζ/R_O is the same for the three datasets. This assumption is justified because it had turned out in preliminary fits, where ζ and R_O had been varied independently, that ζ/R_O was approximately the same for each of the three datasets. A fit to three datasets simultaneously has then 21 variable parameters. The fit result for the sample with a Cr_2O_3 content of 11·5 wt% and measured at 300 K is shown in Fig. 2(c) and numerical values are given in Table 3.

Now there are no problems with the estimation of the errors. We plot the PDFs for both types of Cr atoms separately using these results. Figure 3(c) shows the PDF corresponding to the Cr atoms at regular lattice sites. There are 6·5 Al atoms at ~3·27 Å from the absorbing Cr atoms. The contribution from Cr atoms at random interstitial positions is also shown in Fig. 3(c) for the same sample. The Al peak is modified, according to the model presented here, and there are 10·1 Al atoms about the displaced Cr atoms. The average displacement is $\zeta = 0{\cdot}50$ Å and the ratio ζ/R_O is 0·154 ± 0·007. It is apparent that the radii of the Al coordination shell around the Cr–O octahedra are also about 3·27 Å, just like the Al shell radii for the Cr atoms at regular sites. The number of Al atoms around the interstitial Cr atoms is now much higher than estimated in the previous model, where two Gaussian Al peaks were assumed (10·1 versus 1·8). This difference is possibly

Table 3. Results of a simultaneous fit to three datasets according to the third model

	R_O ΔR_O (Å)	σ_O^2 $\Delta\sigma_O^2$ (10^{-4} Å^2)	N_O ΔN_O	R_{Al} ΔR_{Al} (Å)	σ_{Al}^2 $\Delta\sigma_{Al}^2$ (10^{-4} Å^2)	N_{Al} ΔN_{Al}	$R_{Al} \equiv R_O$ ΔR_{Al} (Å)	ζ $\Delta\zeta$ (Å)	N_{Al} ΔN_{Al}
7·3 wt% 300 K	1·984 ±0·004	38 ±4	6 ±0	3·267 ±0·007	50 ±10	6·5 ±0·9	3·24 ±0·02	0·50 ±0·02	10·1 ±2·4
11·5 wt% 300 K	1·984 ±0·004	37 ±4	6 ±0	3·268 ±0·008	50 ±10	6·5 ±0·9	3·26 ±0·03	0·50 ±0·02	10·1 ±2·4
11·5 wt% 150 K	1·984 ±0·004	32 ±4	6 ±0	3·264 ±0·007	40 ±10	6·5 ±0·9	3·28 ±0·03	0·50 ±0·02	10·1 ±2·4

$\Delta E_O = 0{\cdot}4$ eV ± 1·0 eV; $\Delta E_{Al} = -9{\cdot}1$ eV ± 1·1 eV; $S_0^2 = 0{\cdot}76 \pm 0{\cdot}04$.

due in part to the uncertainty of N_{Al} in the previous model.

It should be noted that for the second and third model the small additional contributions to the Fourier transform is resulting from quite different PDFs. In the second model the additional Al coordination shell has only a few atoms (1·8) and therefore the contribution to the EXAFS or its Fourier transform is small. The third model results in a very broad distribution of Al atoms and the corresponding EXAFS is almost averaged out. However, due to the large number of Al atoms (10.1) a finite small contribution to the Fourier transform still remains.

5 Conclusions

The C–Al distances obtained using one Gaussian peak for the PDF of Al appear to be reasonable for Cr atoms located at regular octahedral lattice sites in the mullite structure (Model 1) though a simple fit with one coordination shell does not agree with the measured data sufficiently. In order to improve the fit, an additional Al coordination shell may be considered (Model 2). The error analysis for the data revealed, however, that σ^2_{Al} and N_{Al} for the added coordination shell are not well defined, and therefore this model is not suitable. A better way of improving Model 1 is given by another model, where a displacement of Cr atoms is taken into account (Model 3). In this model, only 21, rather than 23, variable parameters are used, the residual sum of squares, χ^2, is 25% smaller than in the second model, and the parameters are all well defined. We believe that these Cr atoms occur at distorted positions at interstitial lattice sites. For the Cr atoms an average displacement of $\zeta = 0{\cdot}50$ Å is obtained. This value is an approximation because the angular positions of the Al atoms, which influence the amount and direction of the deduced displacement, were not taken into account. A detailed evaluation of crystal structure data and using present EXAFS data of Cr-doped mullite may allow to define possible sites for the interstitial Cr atoms. Favourable sites for an interstitial incorporation of Cr^{3+} into the mullite structure may be O vacancies or the structure channels running parallel to the crystallographic *c*-axis.[7]

Acknowledgements

One of the authors (KRB) acknowledges with thanks the financial support by the Japan Society for the Promotion of Science (JSPS) through a fellowship during which some of this work was carried out. The work was also supported in part by grants from the Australian Research Council. Another author (AK) is grateful for a fellowship from the Japanese Ministry of Education (Monbusho).

References

1. Cameron, W. E., Mullite: a substituted alumina. *Am. Mineral*, **62** (1977) 747.
2. Burnham, C. W., *Crystal structure of mullite*. Carnegie Inst., Washington Yearb, **63** (1964) 223.
3. Saalfeld, H. & Guse, W., *Structure refinement of 3:2-mullite ($3Al_2O_3{\cdot}2SiO_2$)*. Neues Jahrb. Mineral. Monatsh, 1981, p. 145.
4. Angel, R. J. & Prewitt, C. T., Crystal structure of mullite: a re-examination of the average structure. *Am. Mineral.*, **71** (1986) 1476.
5. Gelsdorf, G., Müller-Hesse, H. & Schwiete, H. E., Einlagerungsversuche an synthetischem Mullit und Substitutionsversuche mit Galliumoxid und Germaniumoxid. *Teil II Arch. Eienhüttenwesen*, **29** (1958) 513.
6. Murthy, M. K. & Hummel, F. A., X-ray study of the solid solution of TiO_2, Fe_2O_3 and Cr_2O_3 in mullite ($3Al_2O_32SiO_2$). *J. Am. Ceram. Soc.*, **43** (1960) 267.
7. Rager, H., Schneider, H. & Graetsch, H., Chromium incorporation in mullite. *Am. Mineral.*, **75** (1990) 392.
8. Ikeda, K., Schneider, H., Akasaka, M. & Rager, H., Crystal-field spectroscopic study of Cr-doped mullite. *Am. Mineral.*, **77** (1992) 251.
9. Harris, F. J., On the use of windows for harmonic analysis with the discrete Fourier transform. *Proceedings of the IEEE*, **66** (1978) 51.
10. Bauchspieß, K. R., EXAFS background subtraction using splines. *Physica B*, **208 & 209** (1995) 183.
11. Bauchspieß, K. R., EXAFIT: a curve-fitting program for EXAFS, *Jpn. J. Appl. Phys.*, **32** (Suppl. 32–2) (1993) 131.
12. Rehr, J. J., Albers, R. C. & Mustre de Leon, J., Single scattering curved wave XAFS code, *Physica B*, **158** (1989) 417.
13. Grunes, L. A., Study of the K edges of *3d* transition metals in pure and oxide form by X-ray-absorption spectroscopy, *Phys. Rev.*, **B27** (1983) 2111.
14. Stern, E. A., Theory of EXAFS, in X-ray Absorption, In *Chemical Analysis*, Vol. 92, eds D. C. Koningsberger & R. Prins, Wiley, New York, 1988, Chap. 1, p. 40.
15. Bauchspieß, K. R., Alberding, N. & Crozier, E. D., Comment on simple method for the evaluation of bond length from data. *Phys. Rev. Lett.*, **60** (1988) 468.
16. Bunker, G., Application of the ratio method EXAFS analysis to disordered systems, *Nucl. Instr. and Meth.* **207** (1983) 437.